SENSOR FAULT QUANTIFICATION IN A FLEXIBLE BEAM CONTROL SYSTEM

HENRIQUE M. PAIVA[1], FERNANDA Q. ROSSI[1], MARCO A. Q. DUARTE[2], ROBERTO K. H. GALVÃO[1]

[1]*Div. Eng. Eletrônica, Instituto Tecnológico de Aeronáutica, São José dos Campos, SP, 12228-900, Brasil*
[2]*Depto. Matemática, Universidade Estadual de Mato Grosso do Sul, Cassilândia, MS, 79540-000, Brasil*
E-mails: hmpaiva@pq.cnpq.br, fer.qrossi@gmail.com, marco@uems.br, kawakami@ita.br

Abstract— This paper proposes a method for quantification of sensor faults in a flexible beam control system on the basis of the ratio of root-mean-square (RMS) values of two measured variables (angular displacement and deflection angle). A theoretical investigation of the closed-loop dynamic relationships reveals that the RMS ratio is more closely related to the fault magnitude if the signals are band-limited prior to the analysis. For this purpose, a wavelet filter bank is employed as a convenient form of splitting the measured signals into different frequency bands. The proposed method is validated with actual experimental data of a flexible beam system. By choosing an appropriate decomposition level in the filter bank, a good correlation between alterations in the sensor gain and the ratio of RMS values was obtained ($R^2 = 0.9997$), yielding a substantial improvement with respect to the analysis in the time domain ($R^2 = 0.8587$).

Keywords— Sensor faults; Fault quantification; Flexible beam control system; Wavelet transform.

Resumo— Este artigo propõe um método para quantificação de falhas de sensor em um sistema de controle de haste flexível, com base na razão de valores RMS (*root-mean-square*) de duas variáveis medidas (deslocamento angular e ângulo de deflexão). Por meio de uma investigação teórica das relações de malha fechada, mostra-se que a razão de valores RMS é mais bem relacionada com a magnitude da falha se os sinais forem previamente limitados a uma faixa de frequências. Para esse propósito, um banco de filtros wavelet é empregado como forma conveniente de dividir os sinais medidos em diferentes faixas de frequência. O método proposto é validado com dados experimentais de um sistema de haste flexível. Escolhendo-se um nível de decomposição adequado no banco de filtros, obtém-se uma boa correlação entre as alterações no ganho do sensor e a razão de valores RMS ($R^2 = 0.9997$), com substancial melhoria em comparação com a análise no domínio do tempo ($R^2 = 0.8587$).

Palavras-chave— Falhas de sensor; Quantificação de falhas; Sistema de controle de haste flexível; Transformada wavelet.

1 Introduction

The mechanical design of robotic manipulators usually employs heavy, stiff structures in order to achieve accurate positioning with minimal vibration. However, many applications require the use of lightweight, slender manipulators to facilitate transportation, obtain higher speed and reduce energy consumption, as well as to operate in working environments with restricted space (Shaheed & Tokhi, 2013). Examples include robotic arms used in space vehicles (Xie, Kalaycioglu & Patel, 1997), hard disk drive head-positioning systems (Yan *et al*., 2013), and manipulators for intervention tasks in nuclear applications (Chalfoun *et al*., 2007). In this case, passive or active methods may need to be employed to attenuate vibrations due to the structural flexibility of the system.

Passive methods involve the introduction of mechanical dampers in the flexible structure, whereas active methods rely on the use of vibration measurements in a feedback control scheme (Gervini, Hemerly & Gomes, 2013; Shaheed & Tokhi, 2013; Wang, Gu & Song, 2014). Sensors employed for this purpose include, for example, strain-gages (Gervini, Hemerly & Gomes, 2013), accelerometers (Scattolini & Cattane, 1999), micro-mechanical gyros (Ortel, Wagner & Saupe, 2013), and PZT (lead zirconate titanate) elements (Wang, Gu & Song, 2014). An important issue that arises in this context is the handling of sensor faults. Indeed, a reliable detection and quantification of the fault may be crucial to allow the reconfiguration of the control system, in order to restore system performance and avoid the propagation of the fault (Scattolini & Cattane, 1999). Moreover, by tracking the evolution of a fault over time, it may be possible to predict the remaining useful life of the sensor by using prognosis techniques, in order to schedule a maintenance intervention within a suitable time frame (Vachtsevanos *et al*., 2006).

The present paper is concerned with the quantification of a sensor fault in a flexible beam control system. Devices of this type have been employed in many studies involving the identification and control of flexible structures (Shaheed & Tokhi, 2013; Gervini, Hemerly & Gomes, 2013) as a laboratory-scale representation of more complex systems such as micro-cantilever sensors used in atomic force microscopy, robotic manipulators and civil engineering structures (Pereira *et al*., 2011).

It is assumed that the system operates under closed-loop control for regulation in the presence of external disturbances. The fault under consideration consists of a change in the gain of the sensor employed to measure the deflections of the beam. Even if this change does not lead to closed-loop instability or significant loss of regulation performance, the quantification of the fault may be of value as an early indicator of a complete sensor failure.

The proposed technique employs a ratio of RMS (root-mean-square) values of two measured quantities, which are shown to be related to the sensor gain. A detailed analysis of the fault effect in the closed-loop system dynamics is presented to indicate that such a ratio of RMS values is more closely related to the fault magnitude if a band pass filter is applied to the measurements. For this purpose, a wavelet filter bank is employed as a convenient form of splitting the measured signals into different frequency bands.

The remainder of this paper is organized as follows. Section 2 describes the flexible beam system and the sensor fault under consideration. Section 3 provides a detailed analysis of the fault effect in the closed-loop dynamics. Section 4 presents the proposed method for fault quantification. A brief description of signal decompositions using a wavelet filter bank is provided in Section 5. The experimental results are presented in Section 6 and concluding remarks are given in Section 7.

2 System description

2.1 Flexible beam system

Fig. 1 depicts the system employed in this work. The control task consists of rotating a thin stainless steel beam in the horizontal plane, with suppression of the beam vibrations, which have a fundamental natural frequency of 3 Hz. The beam is clamped to a hub connected to a DC motor through a set of gears. Deflections at the base of the beam are sensed by a strain gage, as shown in the inset.

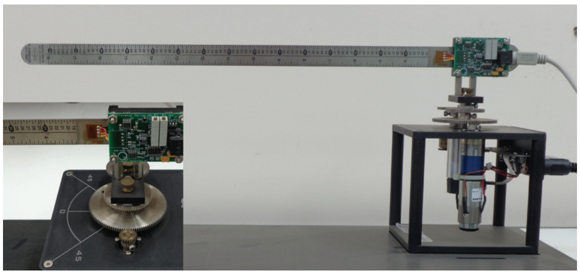

Figure 1. Flexible beam system (Quanser Consulting), with expanded view of the strain gage at the base of the beam.

Fig. 2 presents a schematic diagram of the system, as viewed from the top. The angular displacement of the hub and the deflection of the beam are denoted by θ and α, respectively.

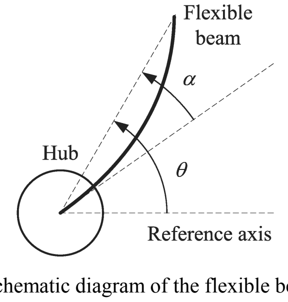

Figure 2. Schematic diagram of the flexible beam system.

In this work, closed-loop control was implemented in the form

$$u = -k_1\theta - k_2\alpha - k_3\dot{\theta} - k_4\dot{\alpha} + d \tag{1}$$

where u is the voltage applied to the motor, d is a disturbance signal and k_1, k_2, k_3, k_4 are feedback gains designed for asymptotically stable operation. The angular displacement θ and the corresponding rate $\dot{\theta}$ are measured by an encoder (1024-line, 4X quadrature) and a tachometer, respectively. The deflection angle α is obtained from the strain-gage readings with suitable calibration. The rate $\dot{\alpha}$ is estimated from α by using a first-order derivative filter. The control law is implemented in a digital computer fitted with a signal acquisition module.

2.2 Sensor fault

The fault under consideration consists of a change in the gain of the strain-gage, which is accomplished by multiplying the actual sensor readings by a coefficient k_f. As a result, the control is calculated as

$$u = -k_1\theta - k_2\alpha_f - k_3\dot{\theta} - k_4\dot{\alpha}_f + d \tag{2}$$

with $\alpha_f = k_f\alpha$. It is implicitly assumed that k_f is such that the closed-loop system remains asymptotically stable. The problem then consists of estimating k_f from the measured signals θ and α_f.

3 Mathematical analysis of the sensor fault

According to the documentation provided by the manufacturer, the dynamics of the flexible beam driven by the DC motor can be described by a state-space model of the form:

$$\begin{bmatrix} \dot{\theta} \\ \dot{\alpha} \\ \ddot{\theta} \\ \ddot{\alpha} \end{bmatrix} = \begin{bmatrix} 0 & 0 & 1 & 0 \\ 0 & 0 & 0 & 1 \\ 0 & a_{32} & a_{33} & 0 \\ 0 & a_{42} & a_{43} & 0 \end{bmatrix} \begin{bmatrix} \theta \\ \alpha \\ \dot{\theta} \\ \dot{\alpha} \end{bmatrix} + \begin{bmatrix} 0 \\ 0 \\ b_3 \\ b_4 \end{bmatrix} u \tag{3}$$

where

$$a_{32} = \frac{K_s}{J_{eq}}, \quad a_{42} = \frac{-K_s(J_{eq} + J_b)}{J_{eq}J_b} \tag{4}$$

$$a_{43} = -a_{33} = \frac{\eta_m \eta_g K_t K_m K_g^2 + B_{eq} R_m}{J_{eq} R_m} \tag{5}$$

$$b_3 = -b_4 = \frac{\eta_m \eta_g K_t K_g}{J_{eq} R_m} \tag{6}$$

For the sake of clarity, the physical meaning of the model parameters is presented in Table 1. However, in what follows, only the general form of the model (3) will be required, along with the relations $a_{43} = -a_{33}$ and $b_3 = -b_4$ expressed in (5) and (6).

Since $a_{33} + a_{43} = 0$ and $b_3 + b_4 = 0$, it follows from (3) that

$$\ddot{\theta} + \ddot{\alpha} = (a_{32} + a_{42})\alpha \tag{7}$$

Table 1. Model parameters.

Parameter	Meaning
K_s	Stiffness constant of the flexible beam
J_{eq}	Equivalent moment of inertia of the motor system as seen at the load
J_b	Moment of inertia of the beam
η_m	Motor efficiency
η_g	Gearbox efficiency
K_t	Motor torque constant
K_m	Motor back electromotive force constant
K_g	Gear ratio
B_{eq}	Equivalent damping coefficient as seen at the load
R_m	Motor armature resistance

It is worth noting that the dynamic relation (7) between the angular displacement θ and the beam deflection α does not involve the input voltage u. In view of (7), a transfer function $G_{\theta\alpha}(s)$ can be written as

$$G_{\theta\alpha}(s) = \frac{\mathrm{A}(s)}{\Theta(s)} = -\frac{s^2}{s^2-(a_{32}+a_{42})} = -\frac{s^2}{s^2+K_s/J_b} \tag{8}$$

where $\Theta(s)$ and $\mathrm{A}(s)$ correspond to the Laplace transforms of $\theta(t)$ and $\alpha(t)$, respectively.

Under the state feedback law (1), the transfer function from the disturbance d to the angular displacement θ is given by

$$G_{d\theta}(s) = \frac{\Theta(s)}{D(s)} = \frac{b_3 s^2 + b_4\overline{a}_{32} - b_3\overline{a}_{42}}{\Delta(s)} \tag{9}$$

where $D(s)$ denotes the Laplace transform of $d(t)$ and $\Delta(s) = s^4 + (k_4 b_4 - \overline{a}_{33})s^3 + (-\overline{a}_{42} - \overline{a}_{33}k_4 b_4 + k_1 b_3 + k_4 b_3 \overline{a}_{43})s^2 + (\overline{a}_{33}\overline{a}_{42} - \overline{a}_{32}\overline{a}_{43})s - k_1 b_3 \overline{a}_{42} + k_1 b_4 \overline{a}_{32}$, with $\overline{a}_{32} = a_{32} - k_2 b_3$, $\overline{a}_{33} = a_{33} - k_3 b_3$, $\overline{a}_{42} = a_{42} - k_2 b_4$, $\overline{a}_{43} = a_{43} - k_3 b_4$.

The relationship between $D(s)$, $\Theta(s)$ and $\mathrm{A}(s)$ is depicted in block diagram form in Fig. 3a.

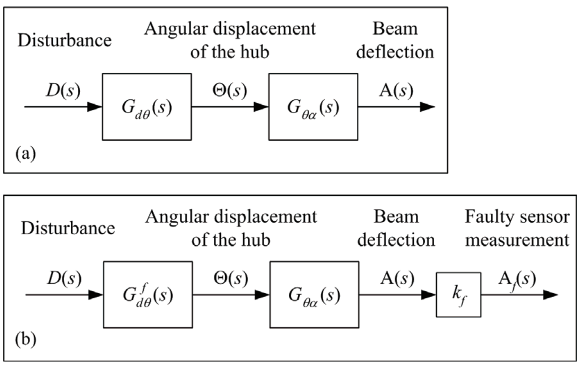

Figure 3. Block diagram of the relationship between disturbance, hub displacement and beam deflection under (a) nominal conditions and (b) sensor fault.

It is worth noting that the closed-loop relations have already been taken into account in the derivation of $G_{d\theta}(s)$, which depends on the feedback gains k_1, k_2, k_3, k_4. The transfer function $G_{\theta\alpha}(s)$ does not depend on these gains, as the dynamic relation (7) between θ and α does not involve the input u.

In the presence of the sensor fault under consideration, the closed-loop dynamics must be derived under the control law (2), with $\alpha_f = k_f\alpha$ representing the faulty sensor measurement employed in the feedback path. Equation (2) can then be rewritten as

$$u = -k_1\theta - k_2^f\alpha - k_3\dot{\theta} - k_4^f\dot{\alpha} + d \tag{10}$$

where $k_2^f = k_2 k_f$ and $k_4^f = k_4 k_f$. The new transfer function from $D(s)$ to $\Theta(s)$ is obtained by replacing k_2 and k_4 with k_2^f and k_4^f, respectively, which leads to

$$G_{d\theta}^f(s) = \frac{b_3 s^2 + b_4\overline{a}_{32}^f - b_3\overline{a}_{42}^f}{\Delta^f(s)} \tag{11}$$

where $\Delta^f(s) = s^4 + (k_4^f b_4 - \overline{a}_{33})s^3 + (-\overline{a}_{42}^f - \overline{a}_{33}k_4^f b_4 + k_1 b_3 + k_4^f b_3\overline{a}_{43})s^2 + (\overline{a}_{33}\overline{a}_{42}^f - \overline{a}_{32}^f\overline{a}_{43})s - k_1 b_3\overline{a}_{42}^f + k_1 b_4 \overline{a}_{32}^f$, with $\overline{a}_{32}^f = a_{32} - k_2^f b_3$ and $\overline{a}_{42}^f = a_{42} - k_2^f b_4$. The transfer function from $\Theta(s)$ to $\mathrm{A}(s)$ remains unaltered, as it does not involve the feedback gains. The relationship between $D(s)$, $\Theta(s)$, $\mathrm{A}(s)$ and $\mathrm{A}_f(s)$ is depicted in Fig. 3b. Again, one should bear in mind that the closed-loop relations are embedded in $G_{d\theta}^f(s)$, which depends on the fault gain k_f.

4 Proposed fault detection method

If the closed-loop system was driven by a sinusoidal disturbance $d(t)$ of frequency ω_0 rad/s, the angular displacement $\theta(t)$ in sinusoidal steady-state would be of the form $\theta(t) = A_\theta \sin(\omega_0 t)$, with phase assumed to be zero without loss of generality. In view of the block diagram in Fig. 3b, the faulty sensor measurements would be given by

$$\alpha_f(t) = A_{\alpha_f}\sin(\omega_0 t + \angle G_{\theta\alpha}(j\omega_0)) \tag{12}$$

with

$$A_{\alpha_f} = k_f\,|G_{\theta\alpha}(j\omega_0)|\,A_\theta \tag{13}$$

Therefore, the fault gain k_f could be simply obtained as

$$k_f = \frac{1}{|G_{\theta\alpha}(j\omega_0)|}\frac{A_{\alpha_f}}{A_\theta} \tag{14}$$

If the disturbance is not sinusoidal, a more elaborate analysis needs to be carried out. More specifically, we will consider the case in which d is a stationary stochastic process with power spectrum density $S_{dd}(\omega)$. In view of Fig. 3b, the power spectrum density of θ can be written as (Papoulis, 1991):

$$S_{\theta\theta}(\omega) = S_{dd}(\omega)\,|G_{d\theta}^f(\omega)|^2 \tag{15}$$

and thus, the variance of θ can be calculated as

$$\sigma_\theta^2 = \frac{1}{2\pi}\int_{-\infty}^{\infty} |G_{d\theta}^f(j\omega)|^2 S_{dd}(\omega)d\omega \quad (16)$$

Similarly, the variance of α_f is given by

$$\begin{aligned}\sigma_{\alpha_f}^2 &= \frac{1}{2\pi}\int_{-\infty}^{\infty} k_f^2 |G_{\theta\alpha}(j\omega)|^2 S_{\theta\theta}(\omega)d\omega \\ &= \frac{k_f^2}{2\pi}\int_{-\infty}^{\infty} |G_{d\theta}^f(j\omega)|^2 |G_{\theta\alpha}(j\omega)|^2 S_{dd}(\omega)d\omega\end{aligned} \quad (17)$$

From (16) and (17), it follows that

$$k_f = \frac{\sigma_{\alpha_f}}{\sigma_\theta}\sqrt{\frac{\int_{-\infty}^{\infty} |G_{d\theta}^f(j\omega)|^2 S_{dd}(\omega)d\omega}{\int_{-\infty}^{\infty} |G_{d\theta}^f(j\omega)|^2 |G_{\theta\alpha}(j\omega)|^2 S_{dd}(\omega)d\omega}} \quad (18)$$

At this point, an inconvenience lies in the dependence of $G_{d\theta}^f(j\omega)$ on k_f, which hampers the use of (18) for direct calculation of k_f. An alternative consists of the use of a band-pass filter to restrict the analysis to a range of frequencies $[\omega_1, \omega_2]$ were $|G_{\theta\alpha}(j\omega)|$ can be approximated by a constant C. In this case, k_f would be approximately given by

$$\begin{aligned}k_f &= \frac{\sigma_{\alpha_f,bp}}{\sigma_{\theta,bp}}\sqrt{\frac{2\int_{\omega_1}^{\omega_2} |G_{d\theta}^f(j\omega)|^2 S_{dd}(\omega)d\omega}{2\int_{\omega_1}^{\omega_2} |G_{d\theta}^f(j\omega)|^2 |G_{\theta\alpha}(j\omega)|^2 S_{dd}(\omega)d\omega}} \\ &\approx \frac{\sigma_{\alpha_f,bp}}{\sigma_{\theta,bp}}\sqrt{\frac{2\int_{\omega_1}^{\omega_2} |G_{d\theta}^f(j\omega)|^2 S_{dd}(\omega)d\omega}{2\int_{\omega_1}^{\omega_2} |G_{d\theta}^f(j\omega)|^2 C^2 S_{dd}(\omega)d\omega}} = \frac{1}{C}\frac{\sigma_{\alpha_f,bp}}{\sigma_{\theta,bp}}\end{aligned} \quad (19)$$

where $\sigma_{\alpha_f,bp}$ and $\sigma_{\theta,bp}$ are the standard deviations of α_f and θ after the band-filtering operation.

In the present work, the band-pass filtering is carried out by using a wavelet filter bank. Experimental data are employed to fit a linear relation between the ratio of standard deviations $\sigma_{\alpha_f,bp}/\sigma_{\theta,bp}$ and the fault gain k_f, as in (19). For this purpose, root-mean-square (RMS) values of the acquired data are used to estimate the standard deviations σ_{α_f} and σ_θ. It is worth noting that the implementation of the proposed technique is carried out in the discrete-time domain, but the main ideas described above remain unaltered.

5 Wavelet filter banks

Fig. 4 presents the basic structure of a wavelet filter bank (Strang & Nguyen, 1996), which is an efficient way of decomposing a signal in different frequency bands. In this figure, y indicates the discrete-time signal of interest, and A_l, D_l denote the corresponding approximation and detail at resolution level l. The transfer functions H(z) and G(z) represent low-pass and highpass wavelet filters, expressed as

$$\mathrm{H(z)} = \sum_{i=0}^{2N-1} h_i z^{-i}, \quad \mathrm{G(z)} = \sum_{i=0}^{2N-1} g_i z^{-i} \quad (20)$$

where z^{-1} is the unit-delay operator and $2N$ is the length of the filter coefficient sequences. The symbol $\downarrow 2$ represents the downsampling operation, which consists of removing every other sample of the signal.

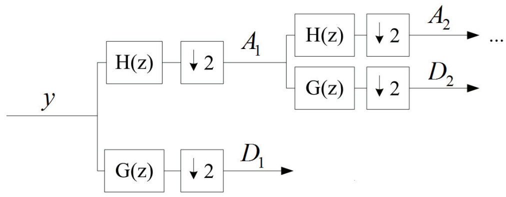

Figure 4. Wavelet filter bank.

The approximation A_l and the detail D_l roughly correspond to the frequency intervals $[0, 2^{-(l+1)}f_s]$ and $[2^{-(l+1)}f_s, 2^{-l}f_s]$, respectively, where f_s denotes the sampling frequency (Strang & Nguyen, 1996). The degree of spectral overlapping between the approximations and details at different levels depends on the selectivity of the wavelet filters. The present work adopts the length-8 filters proposed in (Paiva & Galvão, 2012), which were designed with the aim of obtaining improved frequency resolution.

6 Results and discussion

6.1 Experimental settings

The data acquisition and control tasks were carried out by using the Matlab®/Simulink® software environment (The Mathworks) with QUARC® real-time control software (Quanser Consulting). The feedback gains were obtained by using a linear-quadratic regulator design (Franklin, Powell & Emami-Naeini, 2006) with factory settings for the state and control weights. The resulting values were $k_1 = 20.0$, $k_2 = -93.8$, $k_3 = 3.38$, $k_4 = 0.89$. The continuous-time control law was emulated in discrete time by using a sampling period of 1 ms.

A derivative filter with transfer function $30s/(s + 30)$ was used to estimate the rate $\dot{\alpha}$ from the measurements of α. The disturbance d was generated as the output of a low-pass filter with transfer function $25/(s + 25)$, driven by Gaussian white noise with zero mean and standard deviation of 40. This filter was emulated in discrete time by using the 4th-order Runge-Kutta method with step size equal to the sampling period.

Experimental data were acquired with k_f ranging from 0.5 to 1.5, with 0.1 increments (the nominal condition corresponds to $k_f = 1$). The data for each k_f value were acquired during 120 s. The data were stored at a sampling rate $f_s = 50$ Hz.

6.2 Data analysis

Fig. 5 presents the random disturbance d and the measured values of angular displacement θ and deflection angle α_f, for each fault gain k_f employed in the experiments. The signals are displayed over a 4-second time frame for better visualization.

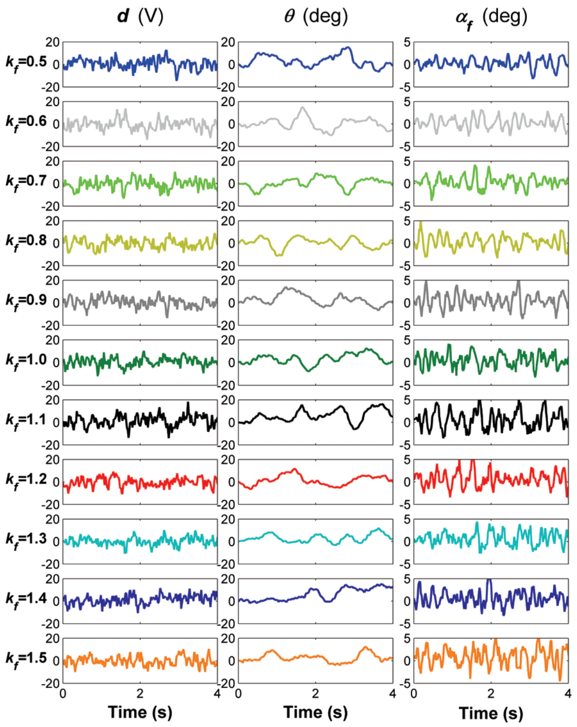

Figure 5. Experimental data (initial 4 seconds).

The standard deviations of α_f and θ were evaluated in the time domain, as well as within different approximation and detail levels of the wavelet decomposition. In order to choose the most appropriate decomposition level for the purpose of fault quantification, linear regression was used to obtain a relation between the fault gain k_f and the ratio $\sigma_{\alpha_f,bp}/\sigma_{\theta,bp}$. The results were compared in terms of the R^2 coefficient (Draper & Smith, 1998), which is a metric usually employed to evaluate the goodness-of-fit, with values close to one indicating a well adjusted model. As shown in Table 3, the best fittings were obtained at the detail levels D_1 (R^2 = 0.9927) and D_2 (R^2 = 0.9997).

Table 3. Linear regression results (R^2).

Decomposition level	Frequency range (Hz)	R^2
Time domain	[0, 25]	0.8587
A_1	[0, 12.5]	0.8368
D_1	[12.5, 25]	0.9927
A_2	[0, 6.25]	0.7763
D_2	[6.25, 12.5]	0.9997
A_3	[0, 3.13]	0.7459
D_3	[3.13, 6.25]	0.9917
A_4	[0, 1.56]	0.9583
D_4	[1.56, 3.13]	0.9477
A_5	[0, 0.78]	0.9535
D_5	[0.78, 1.56]	0.9475

These findings can be interpreted as follows. As discussed in Section 4, the relation between k_f and $\sigma_{\alpha_f,bp}/\sigma_{\theta,bp}$, as expressed by (19), approaches linearity if the analysis is restricted to a range of frequencies where $|G_{\theta\alpha}(j\omega)|$ is approximately constant. In view of (8), $|G_{\theta\alpha}(j\omega)|$ can be written as

$$|G_{\theta\alpha}(j\omega)| = \omega^2 / |-\omega^2 + \omega_0^2| \tag{21}$$

where $\omega_0 = \sqrt{K_s/J_b}$ corresponds to the fundamental natural frequency of the beam (3 Hz). A theoretical plot of $|G_{\theta\alpha}(j\omega)|$ as a function of frequency, as given by (21), is shown in Fig. 6.

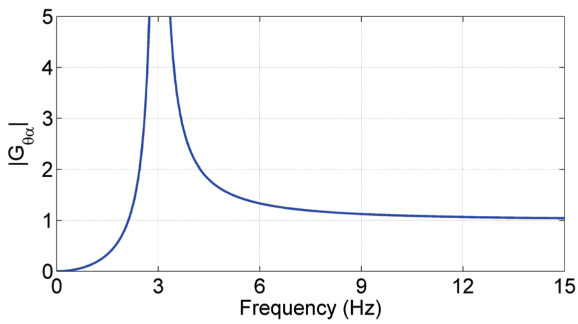

Figure 6. Frequency domain profile of the relation between the magnitudes of angular displacement θ and deflection angle α.

As can be seen in Fig. 6, $|G_{\theta\alpha}(j\omega)|$ tends to one as the frequency increases past 3 Hz, and the curve becomes approximately flat for frequencies larger than 6 Hz. This is the reason why good linearity was obtained at the detail levels D_1 and D_2, which are associated to frequency ranges from 6.25 Hz up to 25 Hz as shown in Table 3. It could be argued that the best result should be obtained at D_1, since the approximation of $|G_{\theta\alpha}(j\omega)|$ by a constant value is best at the highest frequencies. However, the largest R^2 value (0.9997) was actually obtained at D_2, possibly because the corresponding signal-to-noise ratio at this intermediate frequency range (6.25 - 12.5 Hz) is larger compared to the frequency range associated to D_1 (12.5 - 25 Hz).

For illustration, Fig. 7a and Fig. 7b present the relations between $\sigma_{\alpha_f}/\sigma_\theta$ and k_f at the time domain and between $\sigma_{\alpha_f,bp}/\sigma_{\theta,bp}$ and k_f at the detail level D_2. As can be seen, the goodness-of-fit of the linear regression model is substantially improved by using the wavelet decomposition, thus allowing for a much better quantification of the fault if the model was employed to estimate k_f from the ratio $\sigma_{\alpha_f,bp}/\sigma_{\theta,bp}$.

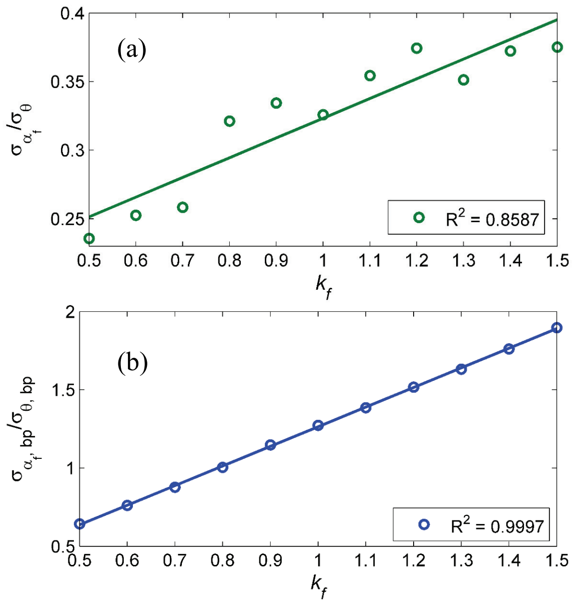

Figure 7. Ratio of standard deviations of the measured variables as a function of k_f at (a) time domain and (b) level-2 detail. The circle markers indicate the experimental points, whereas the straight lines represent the linear regression results.

7 Conclusion

This paper presented a method for quantification of sensor faults in a flexible beam control system on the basis of the ratio of RMS values of two measured variables (angular displacement and deflection angle). These variables can be measured during closed-loop operation, without the need to interrupt the control task. A detailed analysis of the fault effect revealed that such a ratio of RMS values is more closely related to the fault gain if a band pass filter is applied to the measurements. A wavelet filter bank was employed as a convenient form of splitting the measured signals into different frequency bands.

By choosing a convenient decomposition level in the wavelet filter bank, a good correlation between alterations in the sensor gain and the ratio of RMS values was obtained (R^2 = 0.9997), yielding a substantial improvement with respect to the analysis in the time domain (R^2 = 0.8587). This result was also supported by a theoretical analysis of the system dynamics within the frequency bands associated to the wavelet decomposition levels.

Future investigations could be concerned with possible extensions of the proposed technique for real-time detection of faults.

Acknowledgements

The authors acknowledge the support of FAPESP (grant 2011/17610-0), CAPES (Pró-Engenharias MSc scholarship), CNPq (post-doctoral grant 150213/2012-3, doctoral scholarship 140585/2014-1 and research fellowships 303714/2014-0, 300285/2012-4) and FINEP (Captaer and Captaer II grants).

References

Chalfoun, J., Bidard, C., Keller, D., Perrot, Y. and Piolain, G. (2007). Design and flexible modeling of a long reach articulated carrier for inspection, *In Proc. IEEE/RSJ Int. Conf. Intelligent Robots and Systems, San Diego, USA*, pp. 4013-4019.

Draper, N. R. and Smith, H. (1998). *Applied Regression Analysis*, John Wiley, New York.

Franklin, G.F., Powell, J.D. and Emami-Naeini, A. (2006). *Feedback Control of Dynamic Systems*, Prentice Hall, Upper Saddle River.

Gervini, V.I., Hemerly, E.M. and Gomes, S.C.P. (2013). Active control of flexible one-link manipulators using wavelet networks. *Robotica* **31**(8): 1275-1283.

Ortel, T., Wagner, J. F. and Saupe, F. (2013). Integrated motion measurement illustrated by a cantilever beam. *Mechanical Systems and Signal Processing* **34**(1-2): 131-145.

Paiva, H. M. and Galvão, R. K. H. (2012). Optimized orthonormal wavelet filters with improved frequency separation. *Digital Signal Processing* **22**(4): 622-627.

Papoulis, A. (1991). *Probability, Random Variables, and Stochastic Processes*. McGraw-Hill, New York.

Pereira, E., Trapero, J. R., Diaz, I. M. and Feliu, V. (2011). Algebraic identification of the first two natural frequencies of flexible-beam-like structures. *Mechanical Systems and Signal Processing* **25**(7): 2324-2335.

Scattolini, R. and Cattane, N. (1999). Detection of sensor faults in a large flexible structure. *IEE Proceedings - Control Theory and Applications* **146**(5): 383-388.

Shaheed, M.H. and Tokhi, O. (2013). Adaptive closed-loop control of a single-link flexible manipulator. *Journal of Vibration and Control* **19**(13): 2068-2080.

Strang, G. and Nguyen, T. (1996). *Wavelets and Filter Banks*. Wellesley-Cambridge, Wellesley.

Vachtsevanos, G., Lewis, F.L., Roemer, M. and Hess, A. (2006). *Intelligent Fault Diagnosis and Prognosis for Engineering Systems*. John Wiley, New York.

Wang, R. L., Gu, H. and Song, G. (2014). Adaptive robust sliding mode vibration control of a flexible beam using piezoceramic sensor and actuator: An experimental study. *Mathem. Problems in Engineering* **2014**, Article 606817.

Xie, H.P., Kalaycioglu, S. and Patel, R.V. (1997). Control of residual vibrations in the Space Shuttle remote manipulator system. *In Proc. IEEE Int. Conf. Robotics and Automation, Albuquerque, NM,* vol. 4, pp. 2759-2764.

Yan, T. H., He, B., Chen, X. D. and Xu, X. S. (2013). The discrete-time sliding mode control with computation time delay for repeatable run-out compensation of hard disk drives. *Mathem. Problems in Engineering* **2013**, Article 505846.